Structure and magnetism of epitaxially strained Pd(001) films on Fe(001): Experiment and theory

Eric E. Fullerton
Materials Science Division, Argonne National Laboratory, Argonne, Illinois 60439
and Department of Physics, University of California–San Diego, La Jolla, California 92093

D. Stoeffler and K. Ounadjela
Institut de Physique et de Chimie des Matériaux de Strasbourg-(U.M.R. 46 C.N.R.S.), 23 rue du Loess, 67037 Strasbourg, France

B. Heinrich and Z. Celinski*
Physics Department, Simon Fraser University, Burnaby, British Columbia, Canada V5A 1S6

J. A. C. Bland
Cavendish Laboratory, University of Cambridge, Madingley Road, Cambridge CB3 0HE, United Kingdom
(Received 29 August 1994)

We present an experimental and theoretical description of the structure and magnetism of epitaxially strained Pd(001) films on Fe(001) and in Fe/Pd/Fe(001) trilayers. The structure is determined by combining reflection high-energy electron diffraction and x-ray diffraction. For Fe/Au(001) bilayers and Fe/Pd/Au(001) trilayers grown by molecular-beam epitaxy on Ag(001), the Fe and Au layers are well represented by their bulk structure, whereas, thin Pd layers have a face-centered tetragonal structure with an in-plane expansion of 4.2% and an out-of-plane contraction of 7.2% ($c/a=0.89$). Theoretical *ab initio* studies of the interfacial structure indicate that the structural ground state of the epitaxially strained Pd layer is well described by a fct structure which maintains the bulk Pd atomic volume with small deviations at the interface. For Fe/Pd/Fe trilayers, the interlayer coupling oscillates with a period of 4 monolayers (ML) on a ferromagnetic background that crosses to weak antiferromagnetic coupling for thicknesses >12 ML of Pd. Strong ferromagnetic coupling observed below 5 ML of Pd indicates that 2 ML of Pd at each interface are ferromagnetically ordered. Theoretical studies of Fe_3Pd_n superlattices (where n is the number of Pd atomic layers) determine the polarization of the Pd layer and the interlayer magnetic coupling to depend strongly on the c/a ratio of the Pd layers. Modeling of a Pd layer with a constant-volume fct structure and one monolayer interfacial roughness find that the first 2 ML of the Pd is polarized in close agreement with the experimental results. Polarized neutron reflectivity results on an Fe(5.6 ML)/Pd(7 ML)/Au(20 ML) sample determine the average moment per Fe atom of $2.66\pm0.05\mu_B$. Calculations for the same structure show that this value is consistent with the induced Pd polarization.

I. INTRODUCTION

The interface magnetism and interlayer magnetic coupling in the Fe/Pd(001) system is a particularly rich experimental[1–17] and theoretical[13,18–23] problem which has been shown to be strongly dependent on the structural characteristics of the samples. Much of this richness results from the unique properties of Pd which is nearly ferromagnetic with an anomalously large susceptibility. It is well documented that Fe impurities in bulk Pd locally polarize the Pd conduction electrons which couple ferromagnetically with the Fe atoms.[24,25] This results in an effective giant magnetic moment of the Fe atom of order $10\mu_B$ and indirect ferromagnetic exchange of the Fe atoms. The latter giving rise to ferromagnetism for concentrations of Fe impurities as low as 0.1 at. % which has been exploited to study two-dimensional magnetic behavior in relative thick Pd (1.2 at. % Fe) films.[26] Indirect exchange via the Pd atoms is also able to quantitatively explain the ferromagnetic order of submonolayer Fe(001) films on a Pd(001) substrate.[14–16] Similarly, Pd atoms at an Fe/Pd interaface are strongly polarized by the Fe atoms. This polarization has been observed by a number of authors as enhanced magnetic moments in Fe/Pd trilayers and superlattices and strong ferromagnetic interlayer coupling for Pd thicknesses of 4 monolayers (ML) or less.[1–13] Spin-resolved photoemission has observed that the first Pd layer on a Fe(001) substrate is polarized resulting from a hybridization of the Fe-3d/Pd-4d bands.[12,13]

Because of the high density of states at the Fermi surface, the magnetic properties of Pd are sensitive to structural changes. For example, several authors have predicted the onset of ferromagnetism in fcc Pd with a 6% expanded lattice.[27–29] The technique of molecular-beam epitaxy (MBE) makes it possible to explore the interplay of structure and magnetism in thin Pd layers by creating metastable phases and manipulating the atomic structure via epitaxial strains. Original attempts to induce ferromagnetism in Pd was made by epitaxial growth onto Au(001) substrates which gives rise to lateral expansions of the Pd layer.[30] Although long-range ferromag-

netic order was not found, an increase in the susceptibility was observed. In the Fe/Pd(001) system, lattice strains results from the 4.2% mismatch between the bcc Fe (2.866 Å) and fcc Pd ($3.89/\sqrt{2}=2.75$ Å) surface nets. The strained state of the Pd layer will differ depending on growth procedure and sequence. For thin Fe(001) films deposited on Pd(001) substrates, the Fe layer accommodates the strain by lattice matching to the Pd.[17] Conversely, thin Pd(001) films grown on Fe(001) laterally expands to match the Fe.[5] For Pd/Fe(001) superlattices, the strains will depend on the thicknesses of the layers. Several authors have found in different systems such Fe/Pt(001),[31] Mn/Co(0001),[32] and even complex structures such as high-T_c superconductor superlattices[33] that epitaxial strains give rise to tetragonal distortions of the constituent layers.

Structural differences should reflect themselves in the magnetic response of the Pd atoms near the interface and in the interlayer magnetic coupling of across thin Pd layers. Indeed, a large and long-ranged Pd polarization near an Fe/Pd interface can be expected as resulting from the superposition of the proximity effect of the interfacial Fe atoms combined with possible lattice expansions in the Pd. Even if large expansions do not occur in the Fe/Pd systems, a small volume increase resulting from the in-plane matching with Fe can may result in an enhanced polarization.

In this paper we examine the structure, interface magnetism, and interlayer magnetic coupling of epitaxially strained Pd(001) films grown on Fe(001). We present here a detailed description of the structure of this system experimentally as well as theoretically. We have performed a theoretical *ab initio* study of the Fe/Pd interfacial structure by total energy minimization. We have determined the interplanar distances near the Fe/Pd interface and in the Pd spacer which gives the lowest energy. Using this structure, the magnetic moment polarization and interlayer coupling are considered for the case Fe_3Pd_n superlattices for increasing n values. Both the structure and magnetic properties are found to be in good agreement with the experimental results.

This paper is organized as follows. Section II describes the growth and *in situ* reflection high-energy electron diffraction (RHEED) to determine the in-plane structure of Pd(001) layers grown on Fe(001). Section III describes *ex situ* extended x-ray reflectivity to determine the out-of-plane structure. Combining this technique with RHEED allows the atomic volume and tetragonal distortions of thin Pd(001) films grown on Fe(001) to be quantitatively determined. In Sec. IV, the structure of the Fe/Pd systems is determined using first-principles calculations. The determination of the structural parameters focus on the role of tetragonal distortions which minimize the total energy. Section V describes the magnetic properties of the Fe/Pd systems determined by means of ferromagnetic resonance (FMR), Brillouin light scattering, surface magneto-optic Kerr effect (SMOKE), and polarized neutron reflection. The experimental magnetic results are then compared in Sec. VI with *ab initio* theoretical calculations. Section VII summarizes our major conclusions.

II. GROWTH AND IN SITU STRUCTURAL CHARACTERIZATION

A series of Fe(001) films, Fe/Pd(001) bilayers, and Fe/Pd/Fe(001) were grown by MBE techniques onto Ag(001) substrates and capped with 20 ML Au(001) layers where ML is monolayers.[1–9] The bcc Fe(001) layer is lattice matched to the Ag(001) surface net ($4.086/\sqrt{2}=2.89$ Å) to better than 1% and provides a suitable template for the growth of thin bcc Fe(001) films. The details of the growth are presented in detail previously.[5] To briefly summarize, the epitaxial growths were carried out in the low 10^{-10}-Torr range with the Ag substrate held at room temperature. The thickness of each layer is monitored by RHEED intensity oscillations. The in-plane lattice spacing, also determined by RHEED, of the Fe(001) layer is found to relax from that of Ag to the expected bulk Fe spacing after 6 ML. The in-plane lattice spacing of the Pd layers were found to be identical to the Fe(001) surface indicating coherent growth and an in-plane expansion of the Pd layer of 4.2%.

III. X-RAY DIFFRACTION

The out-of-plane structure of the layers were studied *ex situ* by specular x-ray diffraction (XRD). The θ-2θ XRD spectra were obtain on a Rigaku rotating anode diffractometer using Cu K_α radiation over an angular range of $2\theta=1.5$–$75°$. Shown in Fig. 1 are the θ-2θ diffraction spectra for Fe(8.9 ML)/Au(20 ML) and Fe(5.7 ML)/Pd(6.9 ML)/Au(20 ML) samples grown on Ag(001). The intense (002) Bragg peak from the Ag substrate located at 44.34° was deleted for clarity. The contribution of the thin heteroepitaxial layers to the scattered intensi-

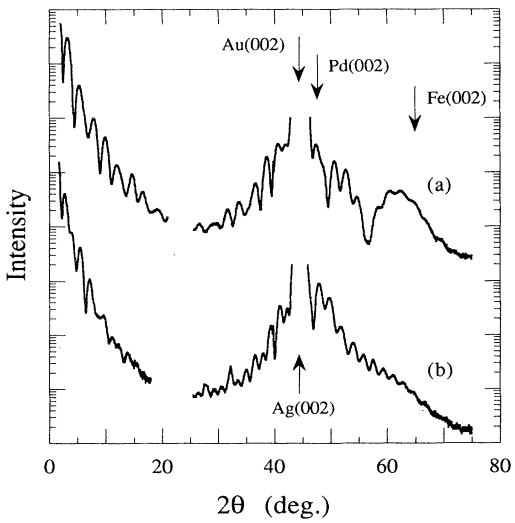

FIG. 1. θ-2θ diffraction results for (a) Ag(001)/Fe(8.9 ML)/Au(20 ML) and (b) Ag(001)/Fe(5.7 ML)/Pd(6.9 ML)/Au(20 ML) samples. The intensity is plotted on a logarithmic scale and the two spectra are offset. The intense (002) Bragg peak from the Ag substrate located at 44.34° is deleted for clarity. Arrows indicate the (002) Bragg positions for bulk Ag, Au, Pd, and Fe.

ty can be seen as oscillation in the intensity between the Ag(00*l*) peaks. The complex diffraction pattern results from interference between the diffracted intensity of the layers and the interference of the layers with the crystal truncation rod of the substrate. In the low-angle reflectivity part of the spectra ($2\theta \approx 1.5-20°$), the scattering vector $q = 4\pi \sin\theta/\lambda$ is much smaller than the characteristic length scale for diffraction $\approx 2\pi/d$, where d is the crystal lattice spacing, and the scattered intensity depends only the average electron density profile of the sample normal to the layers.[34–36] The high-angle part of the spectra is sensitive to diffraction from the lattice spacings of both the layers and the interfaces.[37–42] By fitting the diffracted intensity over an extended range, it is possible to obtain detailed information about the growth morphology, interfacial roughness and lattice strain of thin epitaxial films[34–39] and multilayers.[36,42]

A. Theory

We fitted the low-angle reflectivity data to the standard optical formalism outlined originally by Parrat.[34] To incorporate the effects of interface roughness in the optical formalism we assumed Gaussian interface profiles of width σ, where the Fresnel reflectivity is reduced by a factor $\exp(-2k_1k_2\sigma^2)$ and k_1 and k_2 are the wave vectors above and below the interface.[35,36] We fitted the high-angle data to a kinematic model which includes the lattice spacing of each layer, interface spacings, and discrete monolayer fluctuations in the layer thicknesses and Ag substrate surface.

When the scattering vector is normal to the layer, the one-dimensional (1D) kinematic structure factor for M thin epitaxial layers on a Ag substrate can be written as[37–39,42]

$$F = F_{\mathrm{Ag}} + \sum_{j=1}^{M} \exp(iqz_j) F_j \ , \tag{1}$$

where F_j is the structure factor of the jth layer and z_j is the distance between the top atomic plane of the Ag substrate and the first atomic plane of the jth layer. The scattering factor for the Ag substrate, F_{Ag}, can be approximated as an infinite sum of atomic planes

$$F_{\mathrm{Ag}} = f_{\mathrm{Ag}} \sum_{n=0}^{\infty} \exp(-iqnd_{\mathrm{Ag}}) = f_{\mathrm{Ag}} \frac{1}{1-\exp(-iqd_{\mathrm{Ag}})} \ , \tag{2}$$

where d_{Ag} is the Ag(002) lattice spacing (2.043 Å) and f_{Ag} is the scattering power per unit area of an atomic plane of Ag. The scattering factors for the Fe, Pd, and Au layers, assuming a uniform lattice spacing within the layer, are given by

$$F_j = f_j \frac{1-\exp(iN_jqd_j)}{1-\exp(iqd_j)} \ , \tag{3}$$

where N_j is the number of atomic planes, d_j is the (002) lattice spacing, and f_j is the scattering power per unit area of an atomic plane. A more general expression for F_j is obtained by summing the scattering from each atomic layer with a distribution of lattice spacings to incorporate strain profiles and a distribution of the scattering powers f_j to model interdiffusion. In this paper Eq. (3) will be used to describe the individual layers and the distances z_j in Eq. (1) are given by

$$z_j = d_{0,1} + \sum_{s=1}^{j-1} (N_s - 1)d_s + d_{s,s+1} \ , \tag{4}$$

where $d_{j,j+1}$ is the interface distance between the jth and $(j+1)$th layers.

To include the effects of disorder in the film, we averaged the scattering factor over discrete monolayer fluctuations in the height of the substrate and discrete layer thickness fluctuations. No continuous disorder or interdiffusion is included. To properly model the diffraction data we had to incorporate the fact that the Ag substrate is characterized by a mosaic of single-crystal domains which are slightly misaligned with respect to each other. This can be observed in RHEED and from transverse x-ray-diffraction scans through the Ag(002) Bragg reflection which has a full width at half maximum (FWHM) of $\approx 0.15°$. Therefore, we model the films as having regions which scatter either coherently (within a single-crystal domain) or incoherently (from different single-crystal domains) with other regions of the film. The different regions result from random steps in the substrate surface or fluctuations in the individual layer thicknesses. Let us assume that within a coherent domain that L regions scatter coherently. The scattering factor within that coherent domain is then given by

$$F_L = \frac{1}{L} \sum_{k=1}^{L} \exp(iqh_k) \left[F_{\mathrm{Ag}} + \sum_{j=1}^{M} \exp(iqz_{j,k}) F_{j,k} \right] \ , \tag{5}$$

where h_k is the surface height fluctuation of the Ag substrate in the kth region and $F_{j,k}$ is the scattering factor of the jth layer in the kth region. The substrate height fluctuations give rise to phase shifts in the scattered amplitude from different regions of the sample. A similar model was outlined for superlattices[42] and was used successfully to fit the high-angle x-ray-diffraction spectrum from a GaAs/AlAs superlattice grown on a miscut substrate.[43] The scattered intensity from the sample is then given by $\langle F_L F_L^* \rangle$ where the brackets represent an ensemble average over all possible substrate height and layer thickness configurations. Assuming random fluctuations in the substrate heights, and layer thicknesses which are statistically independent (as originally outlined by Hendricks and Teller[44]) greatly simplifies the averaging process and we obtain

$$\langle F_L F_L^* \rangle = \frac{L-1}{L} |\langle \exp(iqh_k) \rangle|^2 \langle F \rangle \langle F^* \rangle + \frac{1}{L} \langle FF^* \rangle \ , \tag{6}$$

where F is defined in Eq. (1). The first term results from averaging the scattering *amplitude* within a coherent domains. For the limiting value $L = \infty$, Eq. (6) reduces to an amplitude average of a single coherent domain. The

second term in Eq. (6) results from averaging the scattered *intensities* from different domains. In some cases, a transverse scan through a Bragg reflection can be separated into a specular and diffuse component and the diffuse scattering can be subtracted out.[36,37] Since the specular component results from long-range in-plane coherent scattering, an amplitude average ($L=\infty$) is appropriate in this case. However, the mosaic spread of the present substrates limits long-range order and subtracting out the diffuse scattering was not possible. Therefore, we used Eq. (6) with an intermediate value of L. Inserting Eq. (1) into Eq. (6) gives the following:

$$\langle F_L F_L^* \rangle = \frac{L-1}{L} |\langle \exp(iqh_k) \rangle|^2 \{ |F_{\mathrm{Ag}}|^2 + 2\,\mathrm{Re}[F_{\mathrm{Ag}}^* \langle F_B \rangle] + |\langle F_B \rangle|^2 \} + \frac{1}{L} \{ |F_{\mathrm{Ag}}|^2 + 2\,\mathrm{Re}[F_{\mathrm{Ag}}^* \langle F_B \rangle] + \langle |F_B|^2 \rangle \} , \tag{7}$$

where Re indicates the real component of the term in the bracket and

$$F_B = \sum_{j=1}^{M} \exp(iqz_j) F_j .$$

The averaged quantities $\langle |F_B|^2 \rangle$ and $\langle F_B \rangle$ for the three-layer system studied in this paper are given by

$$\langle F_B \rangle = \exp(iqd_{0,1})[\langle F_1 \rangle + T_1 \langle F_2 \rangle + T_1 T_2 \langle F_3 \rangle] , \tag{8}$$

$$\langle |F_B|^2 \rangle = \langle |F_1|^2 \rangle + \langle |F_2|^2 \rangle + \langle |F_3|^2 \rangle + 2\,\mathrm{Re}[\langle F_2 \rangle \langle \Phi_1 \rangle + T_2 \langle F_3 \rangle \langle \Phi_1 \rangle + \langle F_3 \rangle \langle \Phi_2 \rangle] . \tag{9}$$

The bracketed terms in Eqs. (8), and (9) are ensemble averages over the individual layers given by

$$\begin{aligned} \langle F_j \rangle &= \sum_i P(N_i) F_j(N_i) , \\ \langle |F_j|^2 \rangle &= \sum_i P(N_i) F_j(N_i) F_j^*(N_i) , \\ \langle \Phi_j \rangle &= \sum_i P(N_i) \exp\{iq[(N_i-1)d_j, + d_{j,j+1}]\} F_j^*(N_i) , \\ T_j &= \sum_i P(N_i) \exp\{iq[(N_i-1)d_j, + d_{j,j+1}]\} , \end{aligned} \tag{10}$$

where $P(N_i)$ is the probability that jth layer has the N_i number of atomic planes, $F_j(N_i)$ is the structure factor of the jth layer with N_i an integer number of atomic planes given by Eq. (3), and the sum is over all possible N_i. A discrete Gaussian centered about the average layer thickness was used for the distribution $P(N_i)$.[42] In the averages given in Eqs. (10) the distributions have to be normalized such that the sum of probabilities equals unity. Similar averages were used in fitting the spectra from superlattices with discrete disorder,[42] and for ErAs films grown on GaAs.[37,38] The substrate-height distribution was a discrete Gaussian distribution given by

$$\langle \exp(iqh_k) \rangle = \frac{\sum_{n=-3}^{3} \exp(iqnd_{\mathrm{Ag}} - n^2/2\sigma^2)}{\sum_{n=-3}^{3} \exp(-n^2/2\sigma^2)} , \tag{11}$$

where σ is the fluctuation amplitude of the substrate surface.

B. Fitting results

The x-ray-diffraction spectra were least-squares fitted to Eq. (6) multiplied by the Lorentz-polarization factor and a constant scaling factor. The following definition was used for χ^2:

$$\chi^2 = \frac{1}{P} \sum_{i=1}^{P} [\ln I_c(i) - \ln I_m(i)]^2 , \tag{12}$$

where I_c and I_m are the calculated and measured x-ray intensities, and P is the number of data points. The low-angle fitting parameters were the individual layer thicknesses and interface widths. The high-angle fitting parameters include the lattice spacings of the Fe, Pd, and Au layers, and interface spacings between the layers, discrete fluctuations of the Ag substrate and layer thicknesses, the average Au layer thickness, and the lateral averaging parameter L. The lateral average best-fit parameter was $L \approx 7$ for the fits shown below. The average Fe and Pd layer thicknesses were not used as fitting parameters but were determined from the growth conditions which were confirmed from the low-angle x-ray reflectivity results. The parameters determined from the fitting results are listed in Table I.

Figure 2 compares the measured diffraction results to model calculations for the Fe(8.9 ML)/Au(20 ML) film. The inset shows the best-fit results to the low-angle x-ray reflectivity using the optical formalism. The Fe and Au thicknesses determined from this fit are $t_{\mathrm{Fe}} = 13.8$ Å and $t_{\mathrm{Au}} = 39.8$ Å. The expected thicknesses from the growth conditions are 13.1 and 40.8 Å, respectively. Figures 2(a) and 2(b) compare the measured high-angle diffraction data with two model calculations. The calculation in Fig.

TABLE I. X-ray-diffraction results for the fits shown in Figs. 2 and 3. The average layer thicknesses are determined from the low-angle reflectivity spectra and are given in Å and ML. The thickness in monolayers is determined from the equation $t=(N-1)d+d_i$, where t is the average layer thickness, N is the thickness in ML, d is the lattice spacing within the layer, and d_i is the average interface spacing. The lattice spacings and layer roughnesses are determined from fitting the high-angle diffraction spectra. The lattices spacings are determined assuming a uniform lattice spacing within the layer. The layer roughnesses are the standard deviation in layer thickness resulting from monolayer fluctuations.

	Ag/Fe(8.9 ML)/Au(20 ML)	Ag/Fe(5.7 ML)/Pd(6.9 ML)/Au(20 ML)
Layer thicknesses		
t_{Fe}	13.8 Å (9.3 ML)	8.6 Å (5.7 ML)
t_{Pd}		12.8 Å (6.7 ML)
t_{Au}	39.6 Å (19.5 ML)	41.9 Å (20.6 ML)
Lattice spacings		
$d_{Ag,Fe}$	1.95±0.10 Å	1.95±0.10 Å
d_{Fe}	1.435±0.010 Å	1.44±0.02 Å
$d_{Fe,Pd}$		1.77±0.10 Å
d_{Pd}		1.805±0.010 Å
$d_{Fe,Au}$ or $d_{Pd,Au}$	1.85±0.10 Å	1.90±0.05 Å
d_{Au}	2.037±0.005 Å	2.034±0.005 Å
Layer roughnesses		
Ag substrate	1.6 Å	1.8 Å
Fe layer	1.4 Å	1.4 Å
Pd layer		1.8 Å
Au layer	2.0 Å	1.6 Å

2(a) assumes no layer roughness, bulk lattice spacings of 1.434 and 2.038 Å for the Fe and Au, respectively, and interface spacings given by an average of the lattice spacings of the adjacent materials. Although the calculation reproduces the qualitative features of the measured spectrum, there are quantitative discrepancies.

Figure 2(b) compares the best-fit results with the measured spectrum which quantitatively reproduces the spectrum. The Fe thickness was set at 9.3 ML to agree with the low-angle fit. The best fit for the Au thickness was 19.5 ML (39.6 Å) in agreement with the low-angle results. The best-fit lattice spacings within the layers were $d_{Fe}=1.435\pm0.010$ Å and $d_{Au}=2.037\pm0.005$ Å, in agreement with the bulk values. The bulk value of the Fe lattice spacing is in agreement with x-ray photoeletron diffraction[45] and Mössbauer[46] studies which found layers of similar thickness to have little or no tetragonal distortions. The interface spacings are $d_{Ag,Fe}=1.95\pm0.10$ Å and $d_{Fe,Au}=1.85\pm0.10$ Å. In the spectrum, the broad peak centered at $2\theta=61.5°$ results predominantly from the Fe layer. The shift of this peak with respect to the Bragg position of bulk Fe (see Fig. 1) cannot be inferred as a lattice expansion of the Fe layer but results from interference with the Ag substrate and Au capping layer. The high-angle fit also generated a standard deviation in the layer thicknesses resulting from discrete monolayer fluctuations in the layer thicknesses. The best-fit results from the layer roughnesses are 1.6 Å [$\sigma=0.8$ ML in Eq. (12)] for the Ag substrate, 1.4 Å for the Fe layer, and 2.0 Å for the Au layer. These values characterize the layer fluctuations as confined predominantly to ±1 ML about the average thickness.

Figure 3 shows a similar comparison for the Fe(5.7 ML)/Pd(6.9 ML)/Au(20 ML) sample. The inset shows the measured low-angle x-ray reflectivity compared with the best-fit results to the optical formalism. The expected thicknesses from the growth conditions are 8.5, 13.1, and 40.8 Å for the Fe, Pd, and Au layers, respectively. The best fit gives the following average layer thicknesses: $t_{Fe}=8.6$ Å, $t_{Pd}=12.8$ Å, and $t_{Au}=41.9$ Å, in close agreement with the growth parameters. This agreement confirms the layer thickness calibrations which are subsequently used in the high-angle refinement procedure. Figure 3(a) shows the high-angle simulation assuming bulk lattice spacings of 1.434, 1.945, and 2.038 Å for the Fe, Pd, and Au, respectively. Unlike the comparison in Fig. 2(a), the calculation assuming bulk parameters in Fig. 3(a) is qualitatively different from the measured spectrum. In particular, there is a broad feature located at $2\theta\approx60°$ which is not present in the measured spectrum.

Figure 3(b) shows the best-fit results which significantly improve the agreement between the calculated and measured spectrum. The lattice spacings determined from the fitting procedure are $d_{Fe}=1.44\pm0.02$ Å, $d_{Pd}=1.805\pm0.010$ Å, and $d_{Au}=2.034\pm0.005$ Å indicating little change in the Fe and Au spacings and, most dramatically, an $\approx7.2\%$ contraction of the Pd out-of-plane lattice spacing. The interface lattice spacings are $d_{Ag,Fe}=1.95\pm0.10$ Å, $d_{Fe,Pd}=1.77\pm0.10$ Å, and $d_{Pd,Au}=1.90\pm0.05$ Å. The result for d_{Fe} is somewhat dependent on the values for the $d_{Ag,Fe}$ and $d_{Fe,Pd}$ interface values resulting in a larger uncertainty. However, the major result that the Pd lattice spacing is contracted is very robust to changes in the model. The Au thickness was determined to be 20.6 ML (41.9 Å) in agreement with

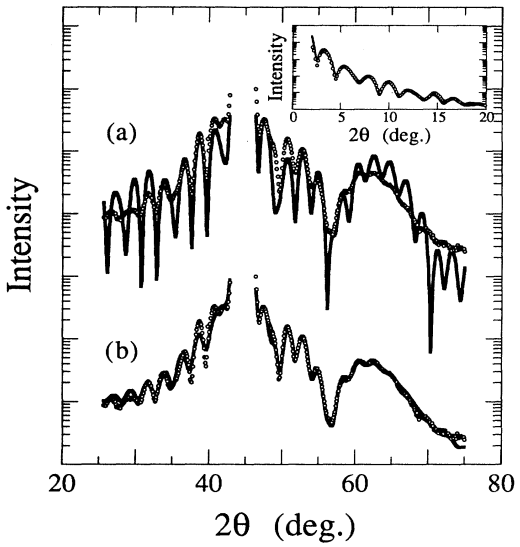

FIG. 2. θ-2θ diffraction results for the Ag(001)/Fe(8.9 ML)/Au(20 ML) sample (open circles) compared with two model calculations (solid lines): (a) assuming bulk lattice spacing and no layer or substrate roughness and (b) best fit to Eq. (7). The inset shows the best fit to the low-angle spectrum. The intensity is plotted on a logarithmic scale and the fitting parameters are described in the text and given in Table I.

the reflectivity result. The best-fit results for the layer roughnesses were 1.8 Å for the Ag substrate, 1.4 Å for the Fe layer, 1.8 Å for the Pd layer, and 1.6 Å for the Au layer. In general, the refined parameters that are common between the two samples are in close agreement giving additional confidence in this approach.

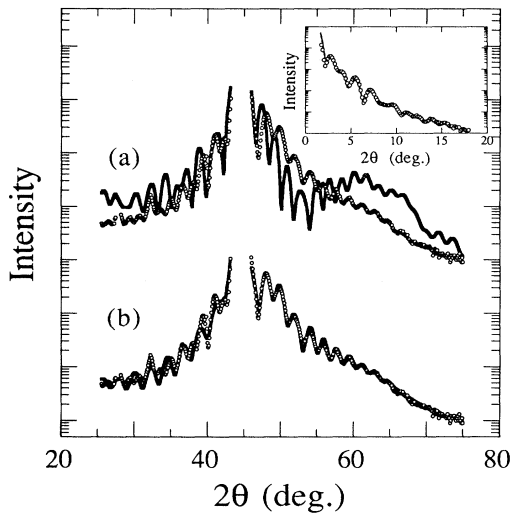

FIG. 3. θ-2θ diffraction results for the Ag(001)/Fe(5.7 ML)/Pd(6.9 ML)/Au(20 ML) sample (open circles) compared with two model calculations (solid lines): (a) assuming bulk lattice spacing and no layer or substrate roughness and (b) best fit to Eq. (7). The inset shows the best fit to the low-angle spectrum. The intensity is plotted on a logarithmic scale and the fitting parameters are described in the text and given in Table I.

The RHEED studies during growth indicate that, in-plane, the Pd layer is expanded to lattice match the Fe surface implying an in-plane lattice strain of $\varepsilon_x = \varepsilon_y = 4.2\%$. We cannot, however, rule out that for samples in which the Pd layer is capped with Au (as opposed to Fe) a small additional strain may arise from the 5.1% lattice mismatch of Au and Pd. The out-of-plane strain determined by XRD is $\varepsilon_z = -7.2 \pm 0.5\%$ indicating that the Pd layer is tetragonally distorted, which can be viewed as either face-centered tetragonal with $a = 2.87\sqrt{2}$ Å, $c = 3.61$ Å ($c/a = 0.89$) or body-centered tetragonal with $a = 2.87$ Å and $c = 3.61$ Å ($c/a = 1.26$). Since the perpendicular component of the stress should vanish in the absence of an external force applied to the film, standard elasticity theory would predict that the perpendicular strain is given by

$$\varepsilon_z = \frac{-2C_{12}}{C_{11}} \varepsilon_x \ , \tag{13}$$

where the Pd values for C_{11} and C_{12} are 224 and 173 GPa, respectively.[47] Equation (13) predicts a perpendicular strain of -6.5%, although some care is needed when applying elasticity theory to ultrathin films with large strains. There are a number of examples in the literature where elasticity theory has not been applicable in ultrathin films.[48–50] Assuming the system maintains constant atomic volume, the perpendicular strain would then be -7.9%. The experimental value for ε_z is slightly larger than the elasticity theory value and indicates that the atomic volume of the Pd is within 1% of the bulk value. Perpendicular contractions of similar magnitude have been found for thin Pt layers on Fe(001) (Ref. 31) and thin Mn layers on Co(111).[32]

IV. FIRST-PRINCIPLES THEORETICAL DETERMINATION OF THE STRUCTURE

Theoretically, the Fe/Pd interface has been mostly studied[20–22] for ultrathin Pd overlayers on an Fe substrate. These studies show that the Pd overlayer exhibits a strong polarization with an interfacial magnetic moment of 0.3 to $0.4\mu_B$. However, it is not possible to apportion the polarization into Fe/Pd interfacial and surface contributions for which the dangling bonds narrows the surface densities of states and favor an enhancement of the surface magnetism. Consequently, these results cannot be directly transposed to sandwich systems. Other theoretical results, using a tight-binding approach,[23] on Fe/Pd sandwiches have exhibited unphysically large ferromagnetic interlayer magnetic couplings between the Fe layers. However, the chosen structural parameters correspond to an expanded Pd structure which is in clear discrepancy with the experimentally determined structure shown above. This highlights the importance of first determining the total-energy minimization of the structure of our system. In addition, the energies involved in structural modifications are usually 2 orders of magnitude larger than those related to magnetic couplings.

In the theoretical part of this paper, our aim is to determine first the equilibrium interfacial atomic struc-

ture using the local-spin-density approximation (LSDA) framework and then to study the main features of the magnetic moments distributions (Sec. VI). We have chosen to use the augmented spherical wave (ASW) method[51] and the LSDA formalism for treating exchange and correlation of a many-electron system which allow to determine the electronic structure of the superlattices. It has been shown recently that this method is well suited to study the interlayer magnetic couplings in various superlattice systems such as Fe/Cr,[52,53] Fe/Mn,[54] Co/Cu,[55] Co/Ru.[56] Detailed descriptions of the technique are given in previous papers.[18,19]

A. Methodolgy

In order to compare theoretical interplanar relaxations with the experimental results, we have determined the crystalline configuration which gives the minimal total-energy value. The total energy for a given crystalline configuration is obtained by a self-consistent calculation of the electronic structure using the *ab initio* ASW technique. Because each self-consistent solution requires extensive computer time and because the total energy results from very complex calculations, the usual minimization techniques cannot been used. In the present work, we determine (i) the total energy for a representative set of structural configurations as a function of one, two, or three variables (the Wigner-Seitz radii) depending on the number of inequivalent Pd atoms (i.e., the Pd layer thickness), (ii) we determine an interpolation of these calculated values with a polynomial function assuming that the energy can be developed as a Taylor polynomial function around the minimal value, and (iii) this function is minimized with respect to the variables. This procedure is an efficient way for the determination of the energy minimum.

It has been shown in Secs. II and III that the Fe lattice is close to the bulk and that the lateral spacing of the Pd layers is identical to the Fe surface, which indicates a lateral expansion of the Pd layer of 4.2%. Consequently, in our calculations, the crystalline structure of the Fe layer is fixed at the experimental bcc structure with a lattice parameter equal to $a_{\mathrm{Fe}}=5.42$ atomic units (a.u.)$=2.867$ Å and the in-plane lattice parameter of the Pd planes is also fixed to this value. Instead of working directly on the interplanar distances, it is more convenient to use the radii $R_{\mathrm{WS}}(i)$ of the Wigner-Seitz spheres (in the atomic sphere approximation) of each nonequivalent atom in the plane i as the real variables in the problem. The interplanar distance between the (001) planes i and $i+1$ is then given by

$$d_{\perp}(P_i-P_{i+1}) = \frac{(4\pi/3)\{[R_{\mathrm{WS}}(i)^3+R_{\mathrm{WS}}(i+1)^3]/2\}}{a_{\mathrm{Fe}}^2} . \quad (14)$$

B. Single-variable minimization of Fe_3Pd_1, Fe_3Pd_2, and Fe_3Pd_7 superlattices

In Fe_3Pd_1 and Fe_3Pd_2, all Pd atoms are equivalent while in Fe_3Pd_7 we assume that all Pd atoms have the same atomic volume (homogeneous relaxations in the Pd spacer). In these three cases, $R_{\mathrm{WS}}(\mathrm{Pd})$ is the only variable in the minimization. Therefore, the Pd-Pd planes interspacing is equal to

$$d_{\perp}(\mathrm{Pd\text{-}Pd})=\frac{(4\pi/3)R_{\mathrm{WS}}(\mathrm{Pd})^3}{a_{Fe}^2}=\frac{c_{\mathrm{Pd}}}{2} \quad (15)$$

and for the Fe-Pd planes interspacing we obtain the average

$$d_{\perp}(\mathrm{Pd\text{-}Fe})=\frac{a_{\mathrm{Fe}}+2d_{\perp}(\mathrm{Pd\text{-}Pd})}{4} . \quad (16)$$

Let us first consider the Fe_3Pd_7 superlattice which is representative of systems with large spacer thicknesses. We use the ferromagnetic (FM) single cell in order to reduce the computation time. Figure 4(c) gives the variation of the total energy for Fe_3Pd_7 in the FM state as a function of the ratio $c_{\mathrm{Pd}}/a_{\mathrm{Fe}}$. The energy minimum is obtained for $R_{\mathrm{WS}}(\mathrm{Pd})$ close to the bulk value $R^0_{\mathrm{WS}}(\mathrm{Pd})$ in agreement with the experimentally determined structure. Previously, we have examined the magnetic properties of Fe/Pd superlattices assuming two model crystalline structures:[18,19] (i) the constant atomic volume (CAV) structure, which is bct, and is obtained assuming that the Pd atoms keep their bulk equilibrium atomic volume and (ii) the expanded atomic volume (EAV) structure for which all Pd atoms have an atomic volume expanded by 13%, the resulting Pd structure being fcc. In both cases, the Pd in-plane lattice spacing is lattice matched to the Fe. The present study shows explicitly that the EAV fcc structure is energetically unstable relative to the tetragonally distorted CAV structure [$E(\mathrm{EAV})-E(\mathrm{CAV})\cong 1.15$ eV]. The latter is representative to the equilibrium structure for large Pd spacers.

Let us now consider smaller Pd thicknesses with Fe_3Pd_1 and Fe_3Pd_2 superlattices. For these two systems, all Pd atoms are stricly equivalent by symmetry. Figures 4(a) and 4(b) give the variation of the total energy for Fe_3Pd_1 and Fe_3Pd_2 superlattices in the AF ground state

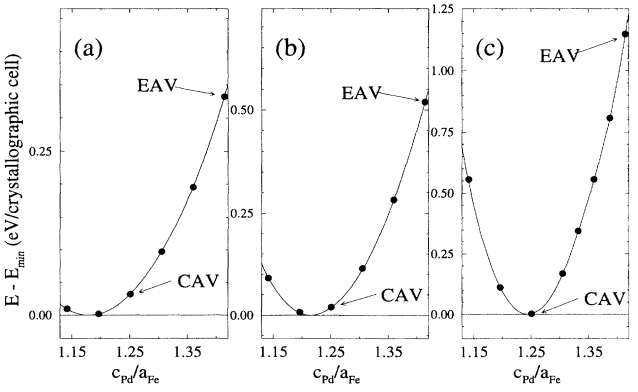

FIG. 4. Total-energy variation as a function of the tetragonal distortion of the Pd spacer structure $c_{\mathrm{Pd}}/a_{\mathrm{Fe}}$ for (a) Fe_3Pd_1, (b) Fe_3Pd_2, and (c) Fe_3Pd_7 superlattices. The arrows indicate the point corresponding to the constant atomic volume (CAV) and the expanded atomic volume (EAV) fcc structures.

(the interlayer magnetic coupling is AF for these Pd thicknesses, see Sec. VI) as a function of the ratio c_{Pd}/a_{Fe}. For Fe_3Pd_1, the energy minimum is obtained for $R_{WS}(Pd)=0.981\times R^0_{WS}(Pd)$ which gives an Fe-Pd interplanar distance equal to $0.545\times a_{Fe}=1.56$ Å. For Fe_3Pd_2, the energy minimum is obtained for $R_{WS}(Pd)=0.991\times R^0_{WS}(Pd)$ which gives an Fe-Pd interplanar distance equal to $0.554\times a_{Fe}=1.59$ Å and a Pd-Pd interplanar distance equal to $0.608\times a_{Fe}=1.74$ Å. For both Pd thicknesses, the energy minima are slightly shifted from the CAV structure, for which the Fe-Pd distance should be equal to $0.5625\times a_{Fe}=1.61$ Å and the Pd-Pd distance equal to $0.625\times a_{Fe}=1.79$ Å.

This study shows that for small Pd thicknesses, the Pd layer is compressed with respect to those obtained for large Pd thicknesses (CAV structure). This indicates that the Fe/Pd interface induces supplementary relaxations to those due to the tetragonal distortion of the CAV structure. This result is obtainable for Fe_3Pd_1 and Fe_3Pd_2 superlattices because the single-variable variation allows one to achieve the complete energy minimization. However, for Fe_3Pd_7 the single-variable variation is only an approximation and may hide relaxations at the interfaces. In order to quantify the variations of these relaxations as a function of the Pd thickness, we perform a complete minimization with 2 and 3 variables for Fe_3Pd_3 and Fe_3Pd_5, respectively.

C. Multivariant minimization of Fe_3Pd_3 and Fe_3Pd_5 superlattices

For these cases, in contrast to Fe_3Pd_1 and Fe_3Pd_2, all Pd atoms are no longer equivalent and the minimization is performed with respect to two values of the Wigner-Seitz radii $R_{WS}(i)$ (interfacial I and central C) in Fe_3Pd_3 and 3 $R_{WS}(i)$ (interfacial I, intermediate $I+1$, and central C) in Fe_3Pd_5. To reduce the computation time, we used the FM single cell. This is a reasonable assumption because the interlayer magnetic coupling becomes very small (5 and 4 meV per crystallographic cell, respectively[18,19]) for these Pd thicknesses.

Figure 5 gives the total energy (in meV) obtained for the Fe_3Pd_3 superlattice for a mesh of interfacial and central Pd R_{WS} values and gives the constant energy lines obtained with the polynomial interpolation. The differences between the second-order polynomial function and the calculated values being <2 meV. This interpolation allows one to obtain an accurate localization of the minimum. The two radii at the minimum are

$$R_{WS}(I,\min)=2.848 \text{ a.u.}\ ,\qquad R_{WS}(C,\min)=2.889 \text{ a.u.}\ , \tag{17}$$

which gives an Fe-Pd interplanar distance equal to $0.554\times a_{Fe}=1.59$ Å and a Pd-Pd interplanar distance equal to $0.622\times a_{Fe}=1.78$ Å. For the CAV case, these distances equal $0.5625\times a_{Fe}=1.61$ Å and $0.625\times a_{Fe}=1.79$ Å, respectively.

Figure 6 gives the total-energy map (in meV) obtained for the Fe_3Pd_5 superlattice as a function of $R_{WS}(I)$, $R_{WS}(I+1)$, and $R_{WS}(C)$. Each node of the 3D mapping in Wigner-Seitz radii space corresponds to a specific total-energy value. The cell for the plane of constant $R_{WS}(C)$ is the same as that surrounded in bold in Fig. 5. By interpolation with a third-order polynomial function, the localization of the minimum is

$$R_{WS}(I,\min)=2.845 \text{ a.u.}\ ,\qquad R_{WS}(I+1,\min)=2.886 \text{ a.u.}\ ,\qquad R_{WS}(C,\min)=2.877 \text{ a.u.}\ , \tag{18}$$

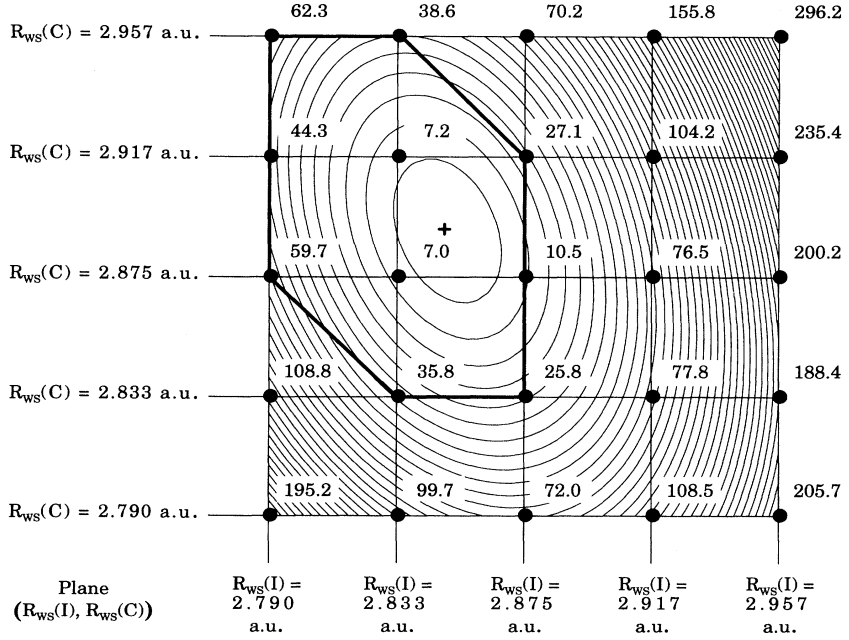

FIG. 5. Plot of the energy difference $E_{tot}-E_{min}$ (in meV) for the values of interfacial (I) and central (C) Pd Wigner-Seitz atoms radii in an Fe_3Pd_3 structure. Each couple $[R_{WS}(I),R_{WS}(C)]$ corresponds to a different Fe_3Pd_3 structure and needs a self-consistent calculation to determine the total energy E_{tot} of this structure. The energy minimum E_{min} corresponds to the minimum of the polynomial function used to fit the total-energy values of the chosen structures. The values of the total energy relative to the minimum ($E_{tot}-E_{min}$) are given for each point of the two-dimensional mesh and the lines correspond to a constant energy value of the polynomial function starting at the minimum value (0 meV) with an increment of 5 meV between successive lines. The crossed point corresponds to the energy minimum [$R_{WS}(I,\min)=2.848$ a.u., $R_{WS}(C,\min)=2.889$ a.u.]. The bold line outlines the plane of constant $R_{WS}(C)$ in Fig. 6.

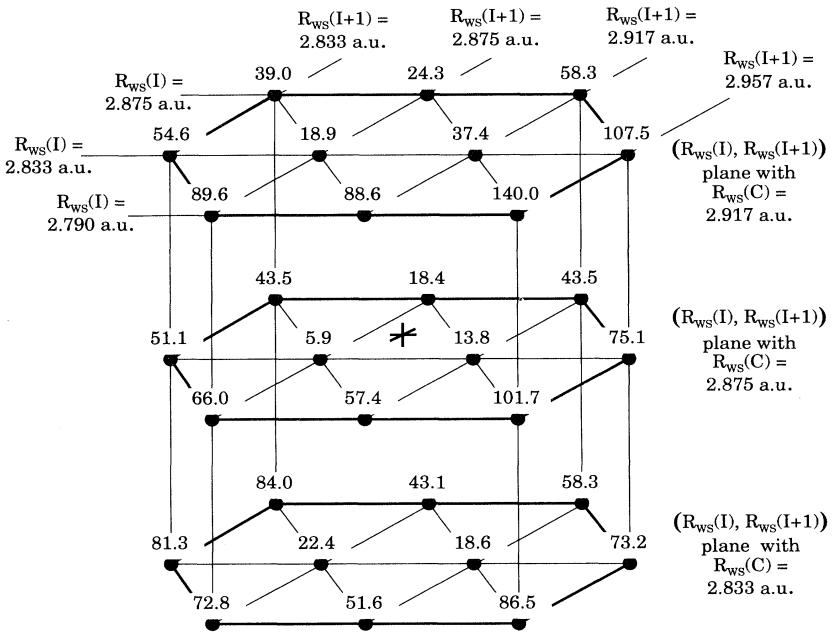

FIG. 6. Plot of the energy difference $E_{tot}-E_{min}$ (in meV) for the values of interfacial (I), inner ($I+1$), and central (C) Pd Wigner-Seitz atoms radii in an Fe_3Pd_5 structure. Each set $[R_{WS}(I),R_{WS}(I+1),R_{WS}(C)]$ corresponds to a different Fe_3Pd_5 structure and needs a self-consistent calculation to determine the total energy E_{tot} of this structure. The energy minimum E_{min} corresponds to the minimum of the polynomial function used to fit the total-energy values of the chosen structures. The values of the total energy relative to the minimum ($E_{tot}-E_{min}$) are given for each point of the three-dimensional mesh. The cell in the plane $[R_{WS}(I),R_{WS}(I+1)]$ corresponds to the outlined domain in Fig. 5 in which the energy minimum is included. The crossed point corresponds to the energy minimum $[R_{WS}(I,\min)=2.845$ a.u., $R_{WS}(I+1,\min)=2.886$ a.u., $R_{WS}(C,\min)=2.877$ a.u.]. The cell for the plane of constant $R_{WS}(c)$ is the same as that surrounded in bold in Fig. 5.

which gives an Fe-Pd interplanar distance equal to $0.553\times a_{Fe}=1.59$ Å, a Pd(I)-Pd($I+1$) interplanar distance equal to $0.619\times a_{Fe}=1.77$ Å and a Pd($I+1$)-Pd(C) interplanar distance equal to $0.629\times a_{Fe}=1.80$ Å. Again, for the CAV structure, these distances equal 1.61, 1.79, and 1.79 Å, respectively.

D. Summary and discussion

Table II summarizes the results obtained for varying the Pd thickness. It shows clearly that, for all of the studied structures, the interplanar distances are close to the ones obtained with the CAV structure. However, a few nuances should be discussed. The interplanar spacing at the Fe-Pd interface is slightly constrained (1.3%) relative to the CAV structure; this contraction is even larger (3.1%) for Fe_3Pd_1, where the proximity effect with the Fe is dominant. This indicates that the calculated contraction at the interface, compared to the inner layers, is robust even for large Pd thicknesses. The contraction decreases rapidly when the proximity effect between Pd and Pd atomic planes becomes predominant: only the first two planes at the interface present an interplanar contraction. Consequently, the CAV structure is a good approximation of the Pd layer ground state and will be used for calculating the interlayer magnetic couplings and the magnetic moments distributions (Sec. VI).

The comparison with the experimental data shows quantitative agreement. The Fe in-plane and perpendicular lattice spacings used for the calculation are found to be close to the bulk values, in agreement with our experimental data. This is an important point because the Fe structure governs the tetragonal distortion of the Pd layer. The calculation determined an interplanar spacing between inner Pd planes (1.803 Å) in agreement with the experimental value 1.805 Å. The tetragonally distorted Pd layer found experimentally and discussed in the preceding section is confirmed by our calculations. This shows that the calculations reproduce the structural properties of the Fe/Pd(001) interface and indicates the correlation between the electronic structure of the material and the local position of the atoms, as reflected by the large energy difference for small atoms displacement.

The experimental results determine that the interfacial Fe-Pd interplanar spacing [$d_\perp$(Fe-Pd)=1.77 Å] is more contracted relative to the inner Pd layers and present the same trend as the calculated results [$d_\perp$(Fe-Pd)=1.59 Å] discussed above. However, the difference between these values is significant. This discrepancy may result from the calculation being performed for perfect interfaces while the interface is experimentally shown to have roughness on the monolayer scale. Interdiffusion, an ordered interfacial compound (e.g, FePd) or lattice matching at step edges will result in increased interface lattice spacing.

TABLE II. Interplanar spacing between Fe-Pd(I), Pd(I)-Pd($I+1$), and Pd($I+1$)-Pd($I+2$) atomic planes. The CAV structure gives the values assuming the Pd layer maintains a constant atomic volume.

	$d_\perp$(Fe-Pd) (Å)	$d_\perp$(Pd-Pd)[1] (I)-($I+1$) (Å)	$d_\perp$(Pd-Pd)[2] ($I+1$)-($I+2$) (Å)
CAV structure	1.61	1.79	1.79
Fe_3Pd_1	1.56		
Fe_3Pd_2	1.59	1.74	
Fe_3Pd_3	1.59	1.78	
Fe_3Pd_5	1.59	1.77	1.80

V. MAGNETIC CHARACTERIZATION

The magnetic properties both of Fe/Pd(001) double layers[1-4] and of Fe/Pd/Fe(001) trilayers[2,5-9] have been studied. The strength of the interlayer exchange coupling through a Pd(001) spacer was quantitatively studied by FMR and Brillouin light scattering. In magnetic trilayers the precessional motions are coupled through the interlayer exchange interaction that results in an acoustic mode in which the magnetic moments precess in-phase and in an optical mode in which the magnetic moments precess out of phase.[2,57] The positions and intensities of both modes depend on the strength of the exchange coupling. The resonance field corresponding to the acoustic mode approaches a value given by the weighted average of the magnetic properties of the two strongly coupled layers. The acoustic mode increases intensity with increasing coupling. With increasing coupling the optical mode decreses in intensity and moves away from the resonance peaks corresponding to uncoupled layers. In the case of ferromagnetic coupling the optical mode originates from that FMR peak, which corresponds to the lower field for zero coupling and with increasing coupling shifts to progressively lower fields.

The thickness dependence of the interlayer exchange coupling at 295 and 77 K is shown in Fig. 7. In ferromagnetically ordered Pd one expects a strong coupling between the Fe layers. Indeed, in Pd layers with the thickness of 4 ML only the acoustic mode was observed, indicating a strong ferromagnetic coupling between the two Fe layers. However one additional atomic layer of Pd decreased the exchange coupling sufficiently so that the optical mode could be observed. The relatively weak coupling through a 5-ML-thick Pd film indicates that only the first 2 ML of Pd at the interface are ferromagnetic as will be discussed in Sec. VI. The temperature dependence of the exchange coupling in the Fe(5.7 ML)/Pd(5 ML)/Fe(9.6 ML) trilayer sample almost exactly follows a Curie-Weiss type of dependence $\sim(1/T)$.[2,5] This behavior can be understood to occur from the presence of fluctuating magnetic moments within the Pd layer which are subjected to the exchange field from the surrounding Fe layers due to RKKY coupling. The Pd atoms can be considered to be Slonczewski's "loose spins."[58] For Pd interlayers thicker than 8 ML, the temperature dependence of the exchange coupling becomes very weak. There is no evidence of fluctuating moments in the Pd(001) layers thicker than 8 ML mediating the interlayer coupling.

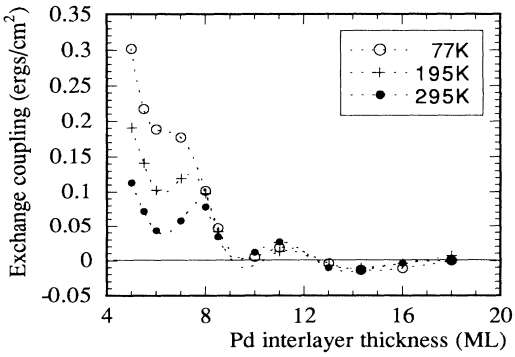

FIG. 7. The thickness dependence of the interlayer exchange coupling J in Ag(001)/Fe(5.7 ML)/Pd/Fe(9.6 ML) trilayer samples. Dashed lines are guides to the eye.

The exchange coupling exhibits a decreasing ferromagnetic background which crosses to AF coupling for thicknesses > 12 ML of Pd. Superimposed on the monotonically decreasing FM background, the oscillatory behavior in the interlayer coupling with increasing Pd thickness is visible, see Fig. 7. The period of oscillation is ~4 ML. This period is close to that predicted for the large Pd Fermi surface 4*d* belly sheets, 3 ML.[29] A similar crossover to AF coupling was originally reported by Schuhl *et al.*[10] for Fe/Pd(001) superlattices on MgO(001). However, more recent studies have determined the coupling to be ferromagnetic over Pd thickness from 4 to 40 Å.[11] A Brillouin light scattering experiment of the coupling in MgO(001)/Fe/Pd/Fe samples preparerd by Childress *et al.*[59] yields ferromagnetic coupling in the range 14–30 Å with a reduction in coupling strength with increasing Pd thickness. The ferromagnetic coupling strength is approximately twice that found for the present samples. This behavior is attributed to the rougher interfaces resulting from growth on MgO substrates. The detailed behavior of the hysteresis loops in Fe/Pd(001) superlattices are sensitive to in-plane anisotropies. Oblique-incidence growth of Fe(001) on MgO substrates induces a weak in-plane uniaxial anisotropy perpendicular to the growth direction.[60] The competition between the fourfold crystalline anisotropy and the twofold uniaxial anisotropy can give the appearance of the antiparallel configuration along certain crystallographic orientations. The SMOKE measurements carried out on Fe/Pd/Fe(001) trilayers grown on the bulk Ag(001) substrates are not affected by in-plane uniaxial anisotropies. The in-plane SMOKE measurements of the individual Fe layers show no measurable in-plane, twofold anisotropy ($H_u < 1$ Oe), and, therefore, the measured crossover to antiferromagnetic coupling in Fe/Pd/Fe(001) trilayer structures is real.

The above results indicate that the Pd(001) grown on Fe(001) rapidly loses its ability to maintain long-range ferromagnetic order. The same conclusion was reached by Rader *et al.*[12,13] as a result of their studies of 1–4 ML of Pd grown on Fe(001). Spin- and angle-resolved valence-band photoemission spectra show that only 1 ML of Pd is ferromagnetically ordered. The thickness dependence of the exchange coupling shows that the Pd magnetic state progresses from the magnetically ordered state ($d_{Pd} < 5$ ML) through the "loose spin configuration" ($d_{Pd} < 8$ ML) to a simple nonmagnetic metallic behavior ($d_{Pd} > 8$ ML).

The transition from strong ferromagnetic coupling with a 4-ML-thick Pd spacer to the presence of the fluctuating magnetic moment in a 5-ML-thick Pd(001) spacer suggests that long-range ferromagnetic order is maintained only in the two Pd(001) atomic layers which are adjacent to the Fe(001). In order to quantify the enhanced moment, polarized neutron reflectivity mea-

surements of the spin asymmetry as a function of reduced wavevector were made below 20 K which is low enough to provide an accurate estimate of the ground-state moment. For the Fe(5.6 ML)/Pd(7 ML)/Au(20 ML) and Fe(5.7 ML)/Pd(8 ML)/Au(42 ML) samples, best-fit values of the average magnetic moment of the layer of $2.66\pm0.05\mu_B$ and $2.6\pm0.2\mu_B$, respectively, are obtained assuming that no induced polarization occurs in the interface Pd layers. In Fig. 8, the spin-asymmetry data for the samples are shown, where the solid and dashed lines correspond, respectively, to the best fit and the bulk moment per Fe atom. The larger error for the measurements on the second sample is due to the increased diffuse scattering resulting from the larger solid angle used in this case and the poorer surface flatness in comparison with the first sample. However, within experimental error, the estimates of the absolute value of the magnetic moment are in agreement for the two investigations. Assuming the Fe has the bulk moment of $2.22\mu_B$, we have an excess moment of $2.5\pm0.3\mu_B$ and $2.2\pm1.1\mu_B$, respectively. Enhanced Fe moments have been predicted[61] (see Sec. VI A) and observed[4,62] for the Ag/Fe interface which needs to be taken into account in order to determine the moment associated with the Fe/Pd interface. Wooten *et al.*[62] estimated the value for the additional moment of $0.65\mu_B$ per interface Fe atom from low-temperature SQUID measurements. This value is comparable with that of $0.84\pm0.14\mu_B$ estimated from polarized neutron reflectivity measurements on noble-metal-coated Ag(001)/Fe layers.[4] Assuming that $0.84\mu_B$ results from the Ag/Fe interface, we deduce that the remaining part (1.66 ± 0.33 and $1.36\pm1.1\mu_B$) is associated with the Fe/Pd interface. These values are reduced from the $3.3\pm1.6\mu_B$ determined in Fe/Pd(001) superlattices.[11] However, this difference most likely results from the enhanced interdiffusion and roughness present in the superlattice samples.

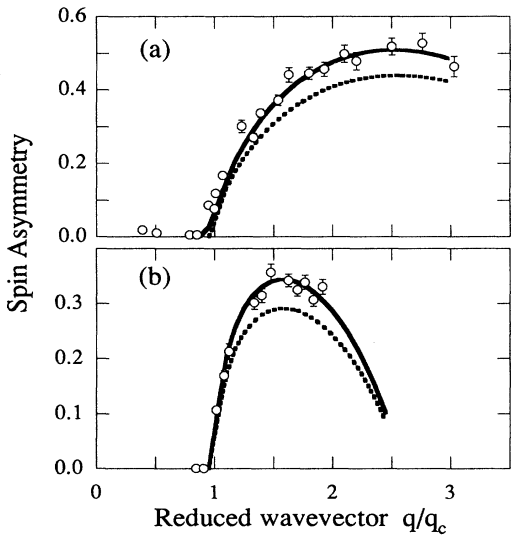

FIG. 8. The corrected neutron spin asymmetry for (a) Ag(001)/Fe(5.6 ML)/Pd(7 ML)/Au(20 ML) and (b) Ag(001)/Fe(5.7 ML)/Pd(8 ML)/Au(42 ML) samples. The dashed lines correspond to the calculated spin asymmetry assuming a bulk Fe moment. The solid line is the best fit to the data giving 2.66 ± 0.05 and $2.6\pm0.2\mu_B$ per Fe atom, respectively.

The presence of ferromagnetic order in the interface atomic layers of Pd(001) is also reflected in the temperature dependence of the total magnetic moment of Fe/Pd(001) layers and the surface anisotropy. The decrease in magnetic moment with increasing temperature is slower in the Fe/Pd system that that observed in Fe/Ag, Au, and Cu structures for comparable Fe thicknesses. The temperature dependence of the total magnetic moment in Fe/Ag, Au, and Cu(001) ultrathin samples can be well described by Bruno's spin-wave theory[63] using the spin-wave gaps which were calculated from the magnetic anisotropies measured by means of FMR.[4] The temperature dependence of the total magnetic moment in the Fe(5.7 ML)/Pd(8 ML) sample is linear in temperature ($\sim10\%$ decrease from 4 to 300 K), but the required spin-wave gap is appreciably larger (1.76 K) than that estimated from the measured magnetic anisotropies (0.34 K). The magnetic moment in Pd appears small and close to that of Ni. The Fe/Ni(001) structures were studied extensively.[2,57,64,65] The Ni(001) growth proceeds in a nearly perfect bcc structure for the first 3–4 atomic layers, then the Ni overlayer undergoes an appreciable lattice reconstruction in which the nearest-neighbor atomic configuration is close to that of fcc Ni. The effective magnetization ($4\pi M_{\rm eff}=9.4$ kG at 300K and 10.7 kG at 77 K) in an Fe(5.7 ML)/Pd(8 ML)/Au(42 ML) film is close to that in an equivalent Fe(5.6 ML)/Ni(3.5 ML) film ($4\pi M_{\rm eff}=8.9$ kG at 300 K and 9.3 kG at 77 K) where the difference in $4\pi M_{\rm eff}$ from the bulk value (21 kG) is a measure of the perpendicular anisotropy. This similar behavior is not common and may result from the similar magnetic and electron properties of Pd with Ni. The perpendicular uniaxial anisotropies in Fe(001) layers which are surrounded only by nonmagnetic layers are significantly larger (e.g., $4\pi M_{\rm eff}=2$ and 1.2 kG in Ag/Fe (5.7 ML)/Ag(001) samples and $4\pi M_{\rm eff}=3.1$ and 1.7 kG in Ag/Fe(5.7 ML)/Cu(001) samples at 300 and 77 K, respectively).

VI. FIRST-PRINCIPLES THEORETICAL DETERMINATION OF THE MAGNETIC PROPERTIES

The theoretical investigation will focus first on the roles of tetragonal distortions and compound formation on the polarization of the interfacial Pd atoms, and then on the interlayer magnetic coupling.

A. Magnetic moments distributions

Figure 9 gives the magnetic moment distributions within the Pd spacer layer for an Fe_3Pd_7 superlattice with perfect interfaces. The results are plotted for various $c_{\rm Pd}/a_{\rm Fe}$ ratios. An increasing $c_{\rm Pd}/a_{\rm Fe}$ has two effects on the magnetic moment distribution: (i) the inner Fe mo-

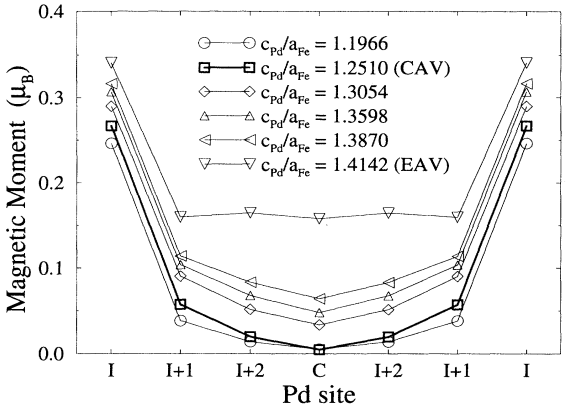

FIG. 9. Magnetic moments distribution in the Pd spacer in an Fe_3Pd_7 structure for various c_{Pd} over a_{Fe} ratio. The interfacial site is denoted by I, the two next planes by $I+1$ and $I+2$, and the inner plane by C.

ments decrease and the interfacial Fe moments increase, and (ii) all Pd magnetic moments for each site increase inducing a long-range Pd polarization for c_{Pd}/a_{Fe} larger than 1.3. The latter result is consistent with previous findings that a 6% lattice expansion of fcc Pd induces ferromagnetism. The curves are similar and exhibit a magnetic moment enhancement on all sites due to the induced polarization by the Fe layer with the polarization decreasing slowly from the interfacial to the inner Pd site. The only exception is for the EAV structure, where the magnetic moments for each inner site (except the interfacial ones) becomes nearly identical exhibiting an intrinsic polarization of the Pd layer.

For the structural ground state, the Pd polarization is mainly induced by the Fe moments and does not have an intrinsic character. The variation of the interfacial magnetic moments indicates that the asymptotic regime for the interfacial properties is already attained for Pd thicknesses larger or equal to 3 atomic planes. In Sec. V, we discussed the Pd polarization determined experimentally. For Fe/Pd/Fe sandwiches, a significant change in the Pd polarization occurs when the Pd thickness is increased from 4 to 5 ML. This result has been explained by the existence of a significant local magnetic moment on the two first interfacial atomic Pd layers. However, the calculated magnetic moment for the second Pd atomic layer is small for the CAV structure ($0.06\mu_B$), as shown in Fig. 9, and cannot be considered as an indication of a polarized plane. Moreover, the neutron data show that the average magnetic moment for the Ag(001)/Fe(5.6 ML)/Pd(7 ML)/Au(20 ML) sample is $2.66\mu_B$. We performed a calculation of the magnetic moment distribution for a similar structure $Ag_5/Fe_5/Pd_6$, assuming a CAV structure for the Pd layer. The results are given in Table III. We find an average magnetic moment of $2.59\mu_B$ per Fe atom (the contribution of the whole Ag, Fe, and Pd layers are $0.034\mu_B$, $12.57\mu_B$, and $0.335\mu_B$, respectively). The Pd polarization is similar to the one calculated for the Fe/Pd superlattice in the CAV structure and stricly located on the first Pd atomic plane. Both

TABLE III. Theoretical magnetic moment distribution for a Ag(5 ML)/Fe(5 ML)/Pd(6 ML) structure. The total moment for the structure is $12.938\mu_B$ which corresponds to an average moment of $2.59\mu_B$ per Fe atom.

Atom in structure	Magnetic moment (μ_B)
Ag	0.0019
Ag	0.0002
Ag	−0.0013
Ag	−0.0045
Ag	0.0373
Fe	2.671
Fe	2.331
Fe	2.406
Fe	2.391
Fe	2.770
Pd	0.262
Pd	0.041
Pd	0.010
Pd	0.006
Pd	0.009
Pd	0.008

points show that the perfect interface modeling of the structure underestimates the polarization of the Pd atoms at the interfaces of our experimental samples. Moreover, fitting of the x-ray data indicates the presence of rough interfaces over one monolayer.

We have extended the calculations to study the role of imperfect interfaces on the Pd polarization for the CAV structures. In this study we used a single ferromagnetic cell to reduce the computation time. The roughness and/or interdiffusion is modeled by introducing compound formation at the interface. In Fig. 10 are

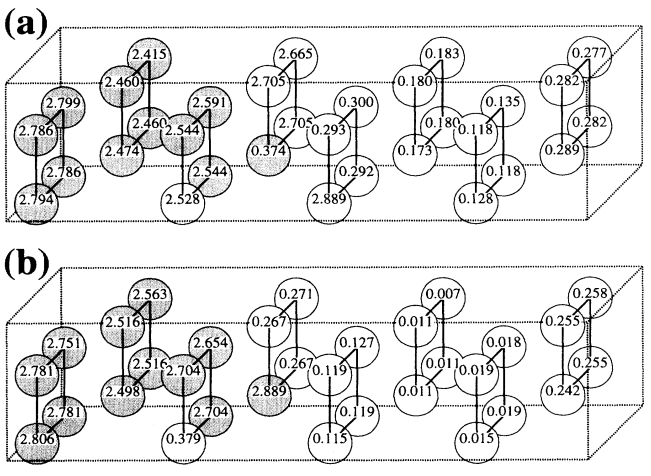

FIG. 10. Magnetic moments distribution (μ_B) in the elemental cell for (a) $Fe_3/Fe_{75\%}Pd_{25\%}/Fe_{25\%}Pd_{75\%}/Pd_3$ issued from the Fe_4Pd_4 superlattices, (b) $Fe_2/Fe_{75\%}Pd_{25\%}/Fe_{25\%}Pd_{75\%}/Pd_4$ issued from the Fe_3Pd_5 superlattices. The Fe atoms are represented in gray and the Pd ones are in white. Lines connect atoms which are in the same atomic plane.

represented our results for Fe_3Pd_5 and Fe_4Pd_4 superlattices with 25% interdiffusion extended over 1 atomic plane about the interface in a (2×2) in-plane cell. The results show the following.

(i) For Fe_3Pd_4 [Fig. 10(a)] the whole Pd layer is polarized with the following average magnetic moments distribution $0.31\mu_B$, $0.18\mu_B$, $0.12\mu_B$, and $0.28\mu_B$ for the 4 Pd planes, which gives a mean magnetic moment of $0.22\mu_B$ per Pd atom.

(ii) For Fe_3Pd_5 [Fig. 10(b)] the whole Pd layer is no longer polarized and 2 planes become nonmagnetic. The average magnetic moments distribution is $0.30\mu_B$, $0.12\mu_B$, $0.01\mu_B$, $0.02\mu_B$, and $0.25\mu_B$ for the 5 Pd planes, which gives a mean magnetic moment of $0.14\mu_B$ per Pd atom. These calculations agree with the experimental results discussed above when we introduce imperfect or mixed interfaces consistent with the structural roughness estimation.

The major result shown by the magnetic moment distributions for 4 and 5 Pd atomic layers is that the second interfacial atomic plane is strongly polarized while the third is almost nonmagnetic. This suggests that the strong ferromagnetic exchange coupling observed for such Pd thickness is related to the Pd polarization. The induced polarization per interfacial atom is found equal to $1.51\mu_B$ (an additional $0.97\mu_B$ over the bulk value coming from the Fe layer and $0.54\mu_B$ from the Pd layer) for these impefect interfaces, in agreement with the experimental value, whereas it is only $1.26\mu_B$ (an additional $0.91\mu_B$ coming from the Fe layer and $0.35\mu_B$ from the Pd layer) when perfect interfaces are considered. Consequently, by adding this enhancement to the Pd contribution in $Ag_5Fe_5Pd_6$, the average magnetic moment per Fe atom increases slightly to $2.64\mu_B$ per Fe atom which agrees with the experimental neutron value. This also suggests that the large polarization ($3.3\pm1.6\mu_B$) (Ref. 11) observed in the Fe/Pd(001) superlattices results from extended interdiffusion of the Fe/Pd interface. As a consequence of the mixed interfacial planes, the Fe-Pd interplanar distance is enhanced as compared to the one obtained for perfet interfaces with $d_\perp$(Fe-Pd)=1.59 Å. The value obtained experimentally of $d_\perp$(Fe-Pd)=1.77 Å is slightly larger and is certainly explained by the mixing at the interface.

B. Interlayer exchange coupling

We determine the interlayer coupling by calculating the difference $\Delta E_{\text{F-AF}}=E_{\text{F}}-E_{\text{AF}}$ between the total energies obtained for the two opposite interlayer magnetic arrangements F and AF. The *F* (AF) interlayer magnetic arrangement corresponds to parallel (antiparallel) magnetizations of successive Fe layers. Figure 11 is a plot of the couplings strength versus Pd spacer thickness. The couplings obtained for the CAV structure oscillates from AF ($n=1,2$) to F ($n=3,4,5$) and back to AF ($n=6$) values. These oscillations can be roughly assimilated to the ones obtained with RKKY theories. In contrast, the couplings obtained for the EAV structure are F, except for $n=1$ resulting from the long-range Pd polarization within the EAV structure as seen in Fig. 9. For the CAV

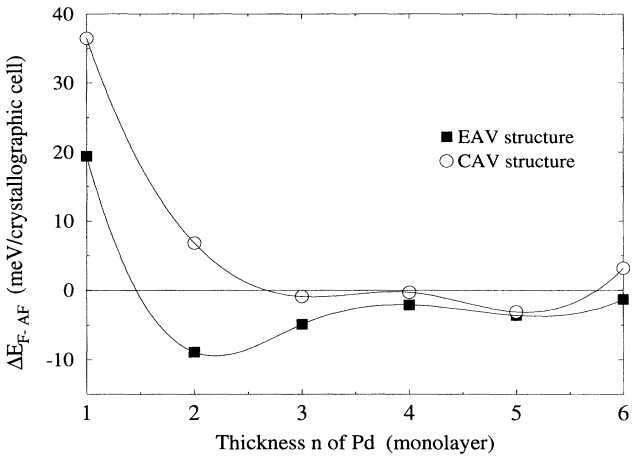

FIG. 11. Interlayer magnetic couplings $\Delta E_{\text{F-AF}}=E_{\text{F}}-E_{\text{AF}}$ in Fe_3Pd_n superlattices as a function of n for the Pd layer having a constant-atomic-volume structure (circles) and for an expanded-atomic-volume fcc structure (squares).

structure, which most closely approximates the experimental structure, the crossover from F to AF is located at 6 ML. The experimental results in Fig. 7 show the interlayer coupling is close to zero for Pd thicknesses ≈9ML and a crossover from F to AF is obtained for a Pd thickness ≈13 ML. This difference with the theoretical data can be understood by the presence of an additional polarization which induces a shift of the crossover to thicker Pd thicknesses. This additional polarization can result from a slight volume expansion of the Pd layer (Fig. 9) and from imperfect interfaces (Fig. 10). Both explanations are in quantitative agreement with the experimental structural results which determined a small ≈1% volume expansion and monolayer-scale interfacial roughness. However, it should be pointed out that the decay of the ferromagnetic coupling is compatible with a Pd polarization localized near the interfaces.

A somewhat surprising result is that the interlayer couplings are positive (i.e., the AF arrangement is the most stable) for the smallest Pd thicknesses ($n=1,2$). This suggests that, for the ferromagnetic arrangement, the polarization of the Pd spacer costs some magnetic moment formation energy which is larger than the energy gain coming from the F interfacial coupling between Fe and Pd layers. These two contributions vanish for the AF arrangement for which the Pd layer is nonmagnetic. This conjecture is consistent with the fact that the weakest AF coupling is obtained for the EAV structure. That is, for large Fe-Pd distances, a given polarization of the Pd atoms costs less energy as a result of the Pd atoms being closer to the Stoner instability. We have also performed the determination of the interlayer coupling as a function of the ratio $c_{\text{Pd}}/a_{\text{Fe}}$ in Fe_3Pd_1 and Fe_3Pd_2 superlattices. This study shows that, for Fe_3Pd_1, the coupling is always positve (AF) and decreases when the interplanar distance is increased. This confirms the stability of this AF coupling. For Fe_3Pd_2, the interlayer magnetic coupling decreases as the interplanar distance is increased and be-

comes negative (F) for a $c_{Pd}/a_{Fe} > 1$ corresponding to the CAV structure. Consequently, for the energy minimum related to the structure (see Sec. IV), the interlayer couplings are AF and are ≈ 50 and 10 meV/crystallographic cell for a Pd thickness of 1 and 2 atomic layers, respectively. This AF coupling is strong and comparable to those found in Co/Ru (0001) superlattices.[56] Unfortunately, no experimental results are available for the 1–2 ML Pd layers studied theoretically. If the interfaces are good enough to avoid the presence of pinholes between the Fe layers, the calculated AF coupling is strong enough to be observable.

VII. CONCLUSIONS

We report an experimental and theoretical investigation of the structural and magnetic properties of epitaxially strained Pd(001) thin films on Fe(001) and in Fe/Pd/Fe(001) trilayers. The in-plane structure is measured by RHEED and the out-of-plane structure by x-ray diffraction. The x-ray-diffraction data is fitted over an extended angular range to determine the average layer thicknesses, perpendicular lattice spacings and interfacial roughnesses. For Fe/Au(001) bilayers and Fe/Pd/Au(001) trilayers epitaxially grown on Ag(001), the Fe and Au layers maintain their bulk structure. The Pd layers have a fct structure with an in-plane expansion of 4.2% and an out-of-plane contraction of 7.2%. Theoretical *ab initio* studies of the interfacial structure indicate that the structural ground state is well described by a fct structure which maintains the bulk Pd atomic volume with small deviations at the interface.

For Fe/Pd/Fe trilayers, the interlayer coupling oscillates with a period of 4 ML on a ferromagnetic background that crosses to weak antiferromagnetic coupling for thicknesses >12 ML of Pd. Strong ferromagnetic coupling observed below 5 ML of Pd indicates that 2 ML of Pd at each interface are ferromagnetically ordered. Polarized neutron reflectivity results on an Fe(5.6 ML)/Pd(7 ML)/Au(20 ML) sample determine an average moment per Fe atom of $2.66 \pm 0.05 \mu_B$ from which we deduce an additional moment of $1.66 \pm 0.33 \mu_B$ per interface Fe atom. Theoretical studies of Fe_3Pd_n superlattices determine the polarization of the Pd layer and the interlayer magnetic coupling to depend strongly on the c/a ratio of the Pd layers. Modeling of a Pd layer with a CAV fct structure and one monolayer interfacial roughness determine that the first 2 ML of the Pd is polarized in close agreement with the experimental result. Modeling of the magnetic interlayer coupling across a CAV Pd layer find the coupling is AF for $n=1$ and 2, F for $n=3-5$, and AF for $n=6$. The experimental results show the interlayer coupling crossover from F to AF is obtained for a Pd thickness ≈ 13 ML. This difference with the theoretical data can be understood by the presence of an additional polarization which induces a shift of the crossover to thicker Pd thicknesses.

These results highlight the interplay of structure and magnetism in the Fe/Pd system. In particular, how structural differences reflect themselves in the magnetic response of the Pd atoms near the interface and in the interlayer magnetic coupling of across thin Pd layers. The polarization and interlayer coupling depends on both the tetragonal distortion of the Pd layer and the interfacial roughness. By incorporating both strain and interfacial roughness in the theoretical treatment of this system, quantitative understanding of the experimental results is obtained.

ACKNOWLEDGMENTS

We would like to thank S. Bader and I. Schuller for helpful discussions. D.S. and K.O. would like to acknowledge J. Sticht for his collabortion in the ASW code and F. Gautier for fruitful discussions. Work at ANL was supported by the U.S. Department of Energy, BES-Materials Sciences, under Contract No. W-31-109-ENG-38. Work at UCSB was supported by DOE Grant No. DE-FG03-87ER45332. Work at SFU was supported by the Natioinal Research Council of Canada. Work at University of Cambridge was supported by EPSRC and the facilities of ILL Grenoble for neutron reflectivity measurements.

*Present address: Optical Sciences Center, University of Arizona, Tuscon, AZ 85721.

[1]B. Heinrich, Z. Celinski, J. F. Cochran, A. S. Arrott, and K. Myrtle, J. Appl. Phys. **70**, 5769 (1991).

[2]B. Heinrich and J. F. Cochran, Adv. Phys. **42**, 523 (1993).

[3]J. A. C. Bland, R. D. Bateson, B. Heinrich, Z. Celinski, and H. J. Lauter, J. Magn. Magn. Mater. **104-107**, 1909 (1992).

[4]J. A. C. Bland, C. Daboo, B. Heinrich, Z. Celinski, and R. D. Bateson, Phys. Rev. B (to be published).

[5]Z. Celinski, B. Heinrich, J. F. Cochran, W. B. Muir, A. S. Arrott, and J. Kirschner, Phys. Rev. Lett. **65**, 1156 (1990).

[6]B. Heinrich, A. S. Arrott, J. F. Cochran, Z. Celinski, and K. Myrtle, in *Science and Technology of Nanostructured Magnetic Materials*, edited by G. C. Hadjipanyasis and G. A. Prinz (Plenum, New York, 1991), p. 15.

[7]W. B. Muir, J. F. Cochran, J. M. Rudd, B. Heinrich, and Z. Celinski, J. Magn. Magn. Mater. **93**, 229 (1991).

[8]Z. Celinski and B. Heinrich, J. Magn. Magn. Mater. **99**, L25 (1991).

[9]Z. Celinski, B. Heinrich, and J. F. Cochran, J. Appl. Phys. **70**, 5870 (1991).

[10]A. Schuhl, J. R. Childress, J. M. George, P. Galtier, O. Durand, A. Barthelemy, and A. Fert, J. Magn. Magn. Mater. **121**, 275 (1993).

[11]J. R. Childress, R. Kergoat, O. Durand, J.-M. George, P. Galtier, J. Miltat, and A. Schuhl, J. Magn. Magn. Mater. **130**, 13 (1994).

[12]O. Rader, C. Carbone, W. Clemens, E. Vescovo, S. Blügel, W. Eberhardt, and W. Gudat, Phys. Rev. B **45**, 13 823 (1992).

[13]O. Rader, E. Vescovo, J. Redinger, S. Blügel, C. Carbone, W. Eberhardt, and W. Gudat, Phys. Rev. Lett. **72**, 2247 (1994).

[14]C. Liu and S. D. Bader, J. Appl. Phys. **67**, 5758 (1990).

[15]C. Liu and S. D. Bader, Phys. Rev. B **44**, 2205 (1991).

[16]K. J. Strandburg, D. W. Hall, C. Liu, and S. D. Bader, Phys.

Rev. B **46**, 10 818 (1992).
[17]J. Quinn, Y. S. Li, H. Li, D. Tian, F. Jona, and P. M. Marcus, Phys. Rev. B **43**, 3959 (1991).
[18]D. Stoeffler, K. Ounadjela, J. Sticht, and F. Gautier, Phys. Rev. B **49**, 299 (1994).
[19]D. Stoeffler, K. Ounadjela, J. Sticht, and F. Gautier, J. Appl. Phys. **75**, 6467 (1994).
[20]S. Blügel, B. Drittler, R. Zeller, and P. H. Dederichs, Appl. Phys. A **49**, 547 (1989).
[21]H. Huang, J. Hermanson, J. G. Gay, R. Richter, and J. R. Smith, Surf. Sci.**172**, 363 (1986).
[22]C. Li, A. J. Freeman, H. J. Hansen, and C. L. Fu, Phys. Rev. B **42**, 5433 (1990).
[23]H. Nait-Laziz, S. Bouarab, C. Demangeat, A. Mokrani, and H. Dreyssé, J. Magn. Magn. Mater. **118**, 365 (1993).
[24]G. J. Nieuwenhuys, Adv. Phys. **24**, 515 (1975).
[25]T. Moriya, *Theory of Magnetism in Transition Metals,* Proceedings of the International School of Physics "Enrico Fermi," Course XXXVII, Varenna, 1967 (Academic, New York, 1967).
[26]D. J. Webb and J. D. McKinley, Phys. Rev. Lett. **70**, 509 (1993).
[27]V. L. Moruzzi and P. M. Marcus, Phys. Rev. B **39**, 471 (1989).
[28]V. L. Moruzzi and P. M. Marcus, Phys. Rev. B **38**, 1613 (1989).
[29]H. Chen, N. E. Brener, and J. Callaway, Phys. Rev. B **40**, 1443 (1989).
[30]M. B. Brodsky and A. J. Freeman, Phys. Rev. Lett. **45**, 133 (1980).
[31]G. W. R. Leibbrandt, R. vanWijk, and F. H. P. M. Habraken, Phys. Rev. B **47**, 6630 (1993).
[32]K. Ounadjela, P. Vennegues, Y. Henry, A. Michel, V. Pierron, and J. Arabski, Phys. Rev. B **49**, 8561 (1994).
[33]E. E. Fullerton, J. Guimpel, O. Nakamura, and I. K. Schuller, Phys. Rev. Lett. **69**, 2859 (1992).
[34]G. Parrat, Phys. Rev. **95**, 359 (1964).
[35]L. Nevot and P. Croce, Rev. Phys. Appl. **15**, 761 (1980).
[36]S. K. Sinha, Physica B **173**, 25 (1991).
[37]P. F. Miceli, C. J. Palmstrøm, and K. W. Moyers, Appl. Phys. Lett. **61**, 2060 (1992).
[38]P. F. Miceli, C. J. Palmstrøm, and K. W. Moyers, Appl. Phys. Lett. **58**, 1602 (1991).
[39]I. K. Robinson, R. T. Tung, and R. Feidenhans'l, Phys. Rev. B **38**, 3632 (1988).
[40]I. K. Schuller, Phys. Rev. Lett. **44**, 1597 (1980).
[41]W. Sevenhans, M. Gijs, Y. Bruynseraede, H. Homma, and I. K. Schuller, Phys. Rev. B **34**, 5955 (1986).
[42]E. E. Fullerton, I. K. Schuller, H. Vanderstraeten, and Y. Bruynseraede, Phys. Rev. B **45**, 9292 (1992).
[43]S. K. Sinha, M. K. Sanyal, S. K.Satija, C. F. Majkrzak, D. A. Neumann, H. Homma, S. Szpala, A. Gibaud, and H. Morkoc, Physica B **198**, 72 (1994).
[44]S. Hendricks and E. Teller, J. Chem. Phys. **10**, 147 (1942).
[45]W. F. J. Egelhoff, I. Jacob, J. M. Rudd, J. F. Cochran, and B. Heinrich, J. Vac. Sci. Technol. A **8**, 1582 (1990).
[46]P. J. Schurer, Z. Celinski, and B. Heinrich, Phys. Rev. B **48**, 2577 (1993).
[47]E. A. Brandes, *Smithells Metals Reference Book* (Butterworths, London, 1983).
[48]M. D. Santis, A. D. Andres, D. Raoux, M. Maurer, M. F. Ravet, and M. Piecuch, Phys. Rev. B **46**, 15 465 (1992).
[49]A. Fartash, M. Grimsditch, E. E. Fullerton, and I. K. Schuller, Phys. Rev. B **47**, 12 813 (1993).
[50]K. Y. Yang, H. Homma, and I. K. Schuller, J. Appl. Phys. **63**, 4066 (1988).
[51]A. R. Williams, J. Küble, and J. C. D. Gelatt, Phys. Rev. B **19**, 6094 (1979).
[52]F. Herman, J. Sticht, and M. V. Schilfgaarde, J. Appl. Phys. **69**, 4786 (1991).
[53]K. Ounadjela, C. B. Sommers, A. Fert, D. Stoeffler, F. Gautier, and V. L. Moruzzi, Europhys. Lett. **15**, 875 (1991).
[54]S. T. Purcell, M. T. Johnson, N. W. E. McGee, R. Coehoorn, and W. Hoving, Phys. Rev. B **45**, 13 064 (1992).
[55]F. Herman, M. V. Schilfgaarde, and J. Sticht, Int. J. Mod. Phys. B **7**, 425 (1993).
[56]D. Stoeffler and F. Gautier, J. Magn. Magn. Mater. (to be published).
[57]B. Heinrich, S. T. Purcell, J. R. Dutcher, K. B. Urquhart, J. F. Cochran, and A. S. Arrott, Phys. Rev. B **38**, 12 879 (1988).
[58]J. C. Slonczewski, J. Appl. Phys. **73**, 5957 (1993).
[59]R. J. Hicken, A. J. R. Ives, D. E. P. Eley, C. Daboo, J. A. C. Bland, J. R. Childress, and A. Schuhl, Phys. Rev. B **50**, 6143 (1994).
[60]Y. Park, E. E. Fullerton, and S. D. Bader (unpublished).
[61]C. L. Fu, A. J. Freeman, and T. Oguchi, Phys. Rev. Lett. **54**, 2700 (1985).
[62]C. L. Wooten, J. Chen, G. A. Mulhollan, J. L. Erskine, and J. T. Markert, Phys. Rev. B **49**, 10 023 (1994).
[63]P. Bruno, Phys. Rev. B **43**, 6015 (1991).
[64]B. Heinrich, A. S. Arrott, J. F. Cochran, K. B. Urquhart, K. Myrtle, Z. Celinski, and Q. M. Zhong, in *Growth, Characterization and Properties of Ultrathin Magnetic Films and Multilayers,* edited by B. T. Jonker, J. P. Heremans, and E. E. Marinero (Materials Research Society, Pittsburgh, PA, 1989), p. 177.
[65]B. Heinrich, J. F. Cochran, A. S. Arrott, S. T. Purcell, K. B. Urquhart, J. R. Dutcher, and J. W. F. Egelgoff, Appl. Phys. A **49**, 473 (1989).